Computational Phase Contrast Magnetic Resonance Imaging Based on Legendre Polynomials

O.M. Dada and O.B. Awojoyogbe

Department of Physics, Federal University of Technology,
P.M.B. 65, Minna, Niger State, Nigeria.

E-mail: awojoyogbe@yahoo.com

Abstract. One of the most exciting modern developments in Magnetic Resonance Imaging (MRI) is the non invasive and non radiation measurements of tissue metabolism in patients. However, different tissue have different hemodynamic responses, which may not be accurately reflected by the general linear model often used in MRI phase contrast measurements or Magnetic Resonance Spectroscopy (MRS). In this study, we have derived analytical expressions for the NMR transverse magnetizations in terms of Legendre Polynomials. We define the orbital angular momentum quantum number as the ratio of the spin lattice relaxation time and the spin-spin relation time. This enables the computation of hemodynamic responses from different tissue quantum mechanically by designating angular momentum states to each biological tissue.

1   Introduction

Phase contrast sequences are the basis of Magnetic Resonance Angiography (MRA) techniques utilizing the change in the phase shifts of the flowing protons in the region of interest to create an image. Spins that are moving along the direction of a magnetic field gradient receive a phase shift proportional to their velocity [1-5]. In a phase contrast sequence, two data sets with a different amount of flow sensitivity are acquired. This is usually accomplished by applying gradient pairs, which sequentially dephase and then rephase spins during the sequence. Both 2D and 3D acquisition techniques can be applied with phase contrast MRA. The first data set is acquired with a flow compensated sequence, that is, without flow sensitivity. The second data set is acquired with a flow sensitive sequence. The amount of flow sensitivity is controlled by the strength of the bipolar gradient pulse pair, which is incorporated into the sequence. Stationary tissue undergoes no effective phase change after the application of the two gradients. Caused by the different spatial localization of flowing blood to stationary tissue, it experiences a different size of the second bipolar gradient compared to the first; the result is a phase shift. The raw data from the two data sets are subtracted. By comparing the phase of signals from each location in the two sequences the exact amount of motion induced phase change can be determined to have a map where pixel brightness is proportional to spatial   velocity.
Phase contrast images represent the signal intensity of the velocity of spins at each point within the field of view (FOV). Regions that are stationary remain black while moving regions are represented as grey to white. The phase shift is proportional to the spin's velocity, and this allows the quantitative assessment of flow velocities. The difference MRI signal has a maximum value for opposite directions. This velocity is typically referred to as venc, and depends on the pulse amplitude and distance between the gradient pulse pair. For velocities larger than venc the difference signal is decreased constantly until it gets zero. Therefore, in a phase contrast angiography it is important to correctly set the venc of the sequence to the maximum flow velocity which is expected during the measurement. However, different blood vessels have

different hemodynamic responses, which may not be accurately reflected by the general linear model often used in current MRI phase contrast measurements [2-4].

In this study, we have derived the analytical expressions for the NMR transverse magnetizations in terms of Legendre Polynomials. The neglect of higher order terms in the current procedure of phase contrast sequence is more of simplifying a difficult mathematical problem with the consequences of loosing very invaluable information about the physiological system under study. Hence, with the advantage of the computational analysis employed in this study, the problems of velocity quantification can be solved with a very minimal or no approximation.

2   Computational Analysis

We study the flow properties of the modified time independent Bloch NMR flow equations which describe the dynamics of hydrogen atom under the influence of radio frequency (RF) magnetic field at Lamour frequency [6-8].

$$f_o = \gamma B - \omega = 0 \tag{1}$$

The x, y, z components (in the rotating frame) of the magnetization of a particle may be given by the Bloch NMR flow equations which may be written as follows [6-8]:

$$\frac{dM_x}{dt} = \frac{\partial M_x}{\partial t} + v \cdot \nabla M_x = -\frac{M_x}{T_2} \tag{2}$$

$$\frac{dM_y}{dt} = \frac{\partial M_y}{\partial t} + v \cdot \nabla M_y = \gamma M_z B_1(x) - \frac{M_y}{T_2} \tag{3}$$

$$\frac{dM_z}{dt} = \frac{\partial M_z}{\partial t} + v \cdot \nabla M_z = \gamma M_z B_1(x) - \frac{M_o - M_z}{T_1} \tag{4}$$

From equations (3) and (4), we obtain the following second order time dependent differential equation which can be solved analytically in Cartesian, Cylindrical and Spherical geometries [6-8].

$$v^2 \frac{\partial^2 M_y}{\partial x^2} + \left(\frac{1}{T_1} + \frac{1}{T_2}\right)v\frac{\partial M_y}{\partial x} + \left(\gamma^2 B_1^{\ 2}(t) + \frac{1}{T_1 T_2}\right)M_y = \frac{M_o \gamma B_1(x,t)}{T_1} \qquad (5)$$

where γ is the gyromagnetic ratio of the fluid particle. The solution presented here is subject to the following two reasonable initial boundary conditions which may conform to the real-time experimental set up:

i) $M_o \neq M_z$, a situation which hold good in general and in particular when the RF $B_1(t)$ field is strong.

ii) Before entering signal detector coil, the soft particle has $M_x = 0$, $M_y = 0$.

iii) $\dfrac{\partial M_y}{\partial t} = 0$.

Under the conditions that when the RF $B_1(x)$ field is applied and the transverse magnetization M_y, has a highest possible magnitude, the equilibrium magnetization $M_0 \approx 0$ [2, 6]. For variable velocity, equation (5) can be written in the form:

$$\frac{d^2 M_y}{dx^2} + \frac{1}{v(x)}\left(T_0 + \frac{dv}{dx}\right)\frac{dM_y}{dx} + \frac{T_g}{v^2(x)}M_y = 0 \qquad (6)$$

The fluid velocity v is dependent on the spatial variable x. We may therefore make the following assumption [6]:

$$\frac{1}{v(x)}\left(T_0 + \frac{dv}{dx}\right) = \frac{1}{l}Cot\frac{x}{l} \qquad (7)$$

where $l = l(x)$ is an experimental parameter and $Cot\dfrac{x}{l}$ is a cotangent function of

$\dfrac{x}{l}$. Equation (6) is based on the condition that:

$$\gamma^2 B_1^2(x) << \frac{1}{T_1 T_2} \qquad (8)$$

where: $T_0 = \left(\dfrac{1}{T_1} + \dfrac{1}{T_2}\right) = \dfrac{(T_1 + T_2)}{T_1 T_2}$, $T_g = \dfrac{1}{T_1 T_2}$ \qquad (9)

Since the expression of equation (7) implies that the fluid velocity is a function of relaxation times, we can assume that v^2 is directly proportional to T_g such that

$$\frac{v^2(x)}{T_g} = \frac{1}{n(n+1)} l^2(x) \tag{10}$$

where $\dfrac{1}{n(n+1)}$ is the constant of proportion (n is a positive integer parameter).

Hence, from equation (10), we can write:

$$\frac{d^2 M_y}{dx^2} + \frac{1}{l} Cot\frac{x}{l} \frac{dM_y}{dx} + \frac{1}{l^2} n(n+1) \, M_y = 0 \tag{11}$$

$$Sin\frac{x}{l} \frac{d^2 M_y}{dx^2} + \frac{1}{l} Cos\frac{x}{l} \frac{dM_y}{dx} + \frac{1}{l^2} Sin\frac{x}{l} n(n+1) M_y = 0 \tag{12}$$

$$\frac{d}{dx}\left(Sin\frac{x}{l} \frac{dM_y}{dx} \right) + \frac{1}{l^2} Sin\frac{x}{l} \, n(n+1) M_y = 0 \tag{13}$$

If we define $\dfrac{x}{l}$ as the phase of the NMR signal and setting $\varepsilon = Cos\dfrac{x}{l}$, we

can obtain a Legendre differential equation from equation (13) as follows:

$$\frac{d}{d\varepsilon}\left[\left(1-\varepsilon^2\right)\frac{dM_y}{d\varepsilon} \right] + n(n+1)M_y = 0 \tag{14}$$

$$\left(1-\varepsilon^2\right)\frac{d^2 M_y}{d\varepsilon^2} - 2\varepsilon\frac{dM_y}{d\varepsilon} + n(n+1)M_y = 0 \tag{15}$$

The solution of equation (15) is of the form [6]:

$$M_{yn}(\varepsilon) = C_1 P_n(\varepsilon) + C_2 Q_n(\varepsilon) \tag{16}$$

where $P_n(\varepsilon)$ and $Q_n(\varepsilon)$ are the Legendre polynomials of the first kind and second kind respectively; C_1 and C_2 are constants. It is worthy of note that $P_n(\varepsilon)$ and $Q_n(\varepsilon)$ are two linearly independent solutions to equation (15). For the transverse magnetization to be finite when x becomes very large C_2 must be equal to zero. Therefore, the final solution is given as:

5

$$M_{yn}(\varepsilon) = C_1 P_n(\varepsilon) \tag{17}$$

Equation (17) represents the NMR transverse magnetization and signals as functions of Legendre polynomials. Traditionally, n is a positive integer which we shall define as follows:

$$n = \frac{T_1}{T_2} \tag{18}$$

Table 1 and figures (1-8) show the values of n for different biological tissues and its corresponding influence on the NMR signals. For the purpose of checking the geometrical behavior of the solutions, we have used integer values to represent n and experimental values for the gradient pulse parameters [6]:

$$\gamma G \tau = \frac{1}{l} \tag{19}$$

| Tissue	$T_1(s)$	$T_2(s)$	$T_0(s^{-1})$	$T_g(s^{-2})$	$n = T_1/T_2$	n (approximate)
CSF[9]	2.50	0.250	4.4	1.6	10	10
White Matter[10]	1.08	0.124	8.990442	7.467145	8.709677	9
Grey Matter[10]	0.92	0.114	9.858886	9.534706	8.070175	8
Kidney[10]	0.83	0.082	13.39994	14.69292	10.12195	10
Liver[10]	0.61	0.057	19.18320	28.76043	10.70175	9
Normal breast fat[11]	0.25	0.060	20.66667	66.66667	4.166667	4
Fibroglandular tissue[11]	0.70	0.080	13.92857	17.85714	8.750000	9
Cancerous lesions[11]	0.80	0.100	11.25000	12.50000	8.000000	8
Cyst [12]	1.068947	0.406918	3.393000	2.298991	2.626937	3
Abscesses [12]	1.212856	0.212436	5.531800	3.881169	5.709278	6

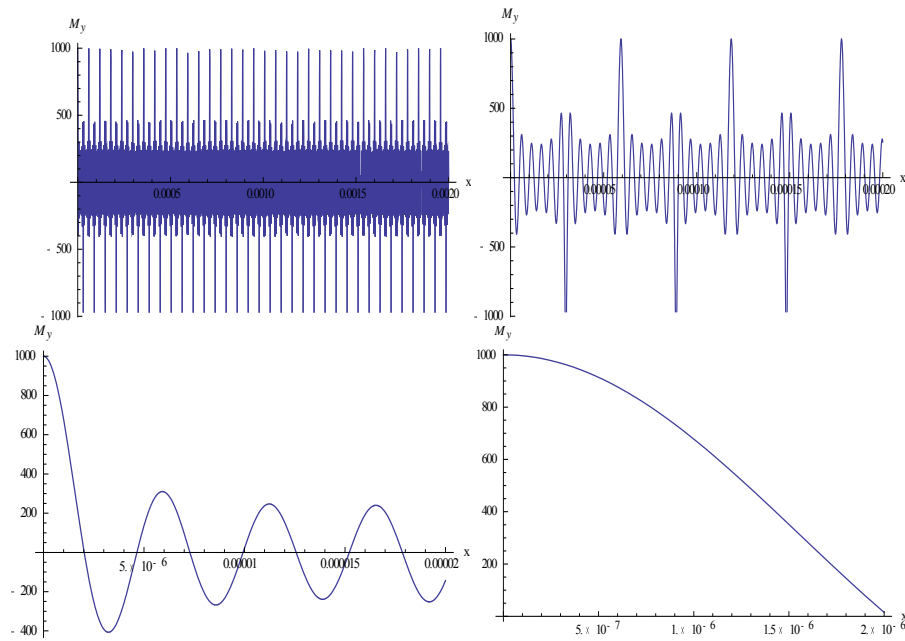**Table 1.** Relaxation times and relaxation rates of different tissues at 1.5T [9-12].
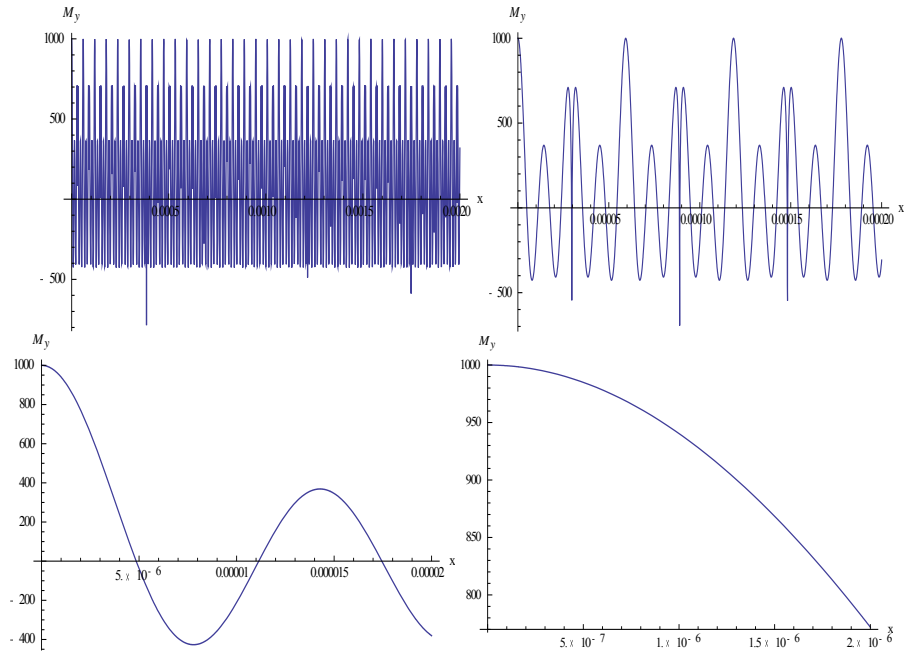
Fig. 1. Plots of M_y against x (for different geometrical ranges) for normal breast fat [11] at 1.5T: $C_1 = 1000$, $G = 0.2 \mathrm{Tm}^{-1}$, $\tau = 2 \mathrm{ms}$.
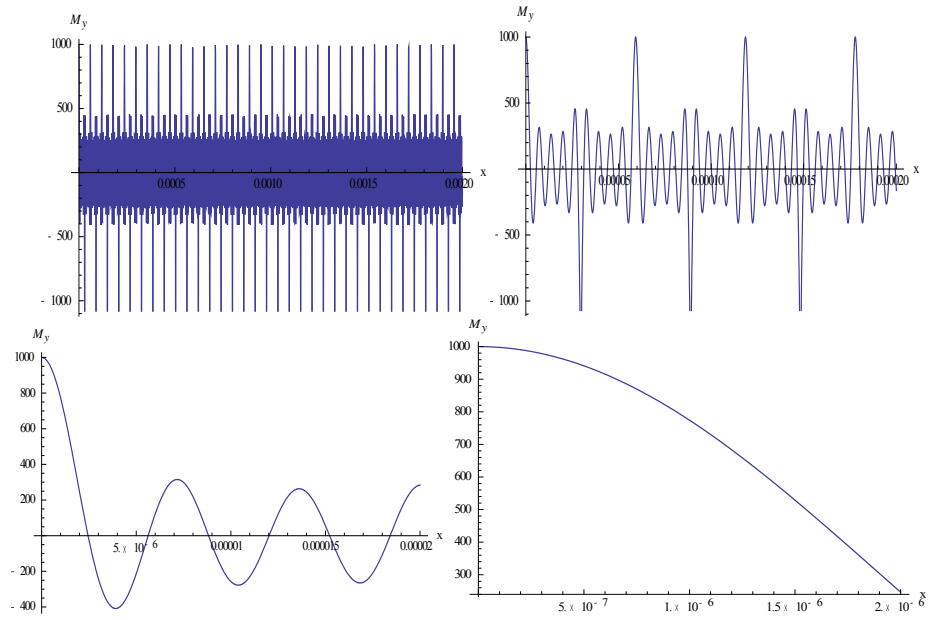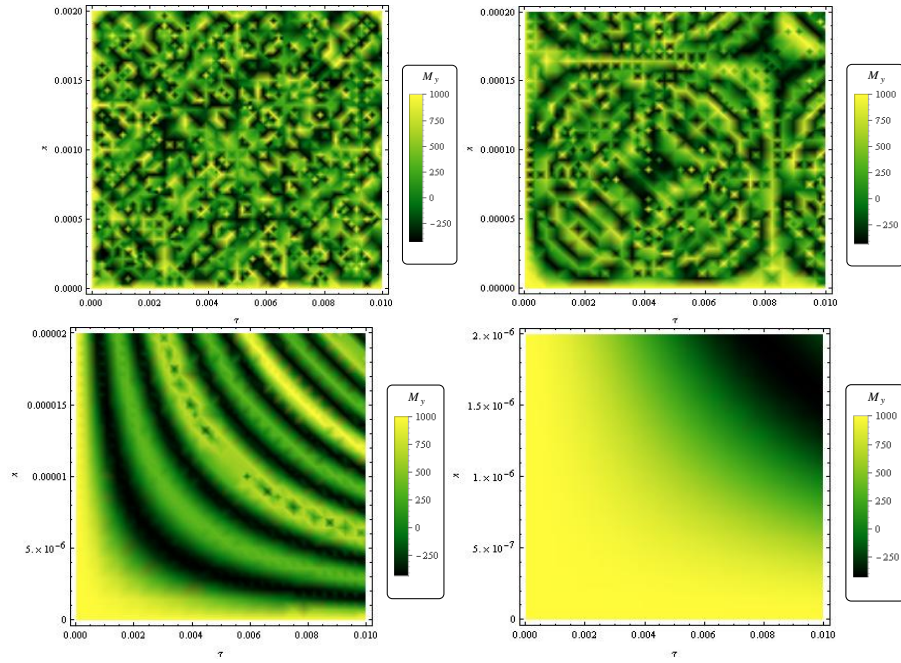
Fig. 2. Plots of M_y against x (for different geometrical ranges) for fibroglandular tissue [11] at 1.5T: $C_1 = 1000$, $G = 0.2Tm^{-1}$, $\tau = 2ms$.
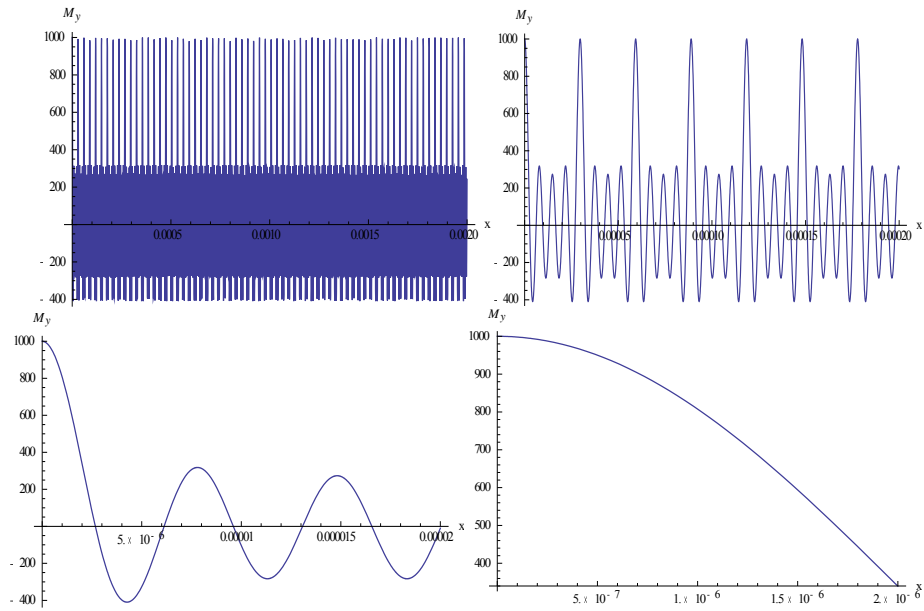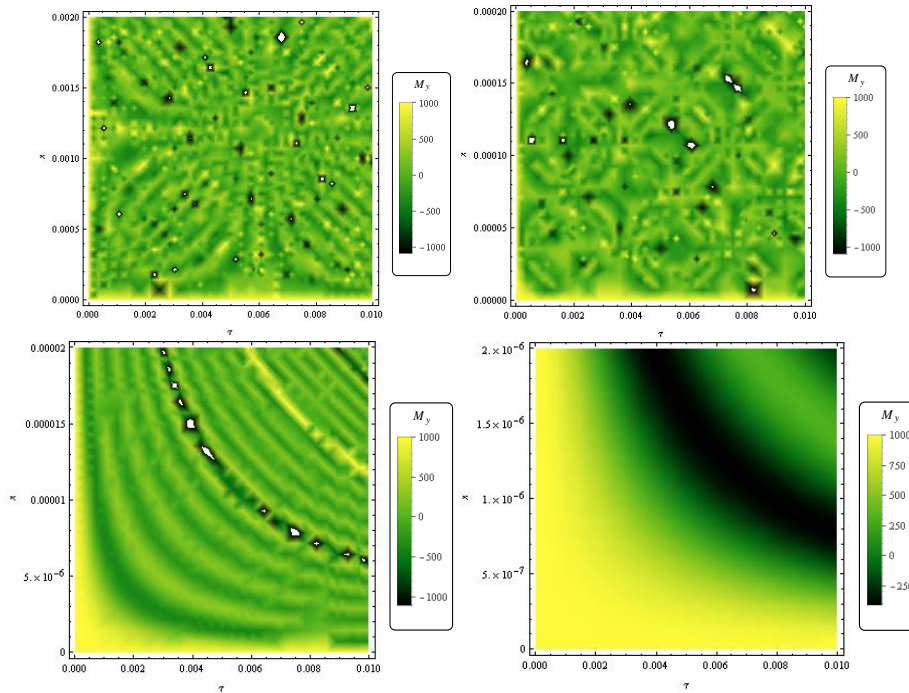
Fig. 3. Plots of M_y against x (for different geometrical ranges) for cancerous lesions [11] at 1.5T: $C_1 = 1000$, $G = 0.2 Tm^{-1}$, $\tau = 2ms$.
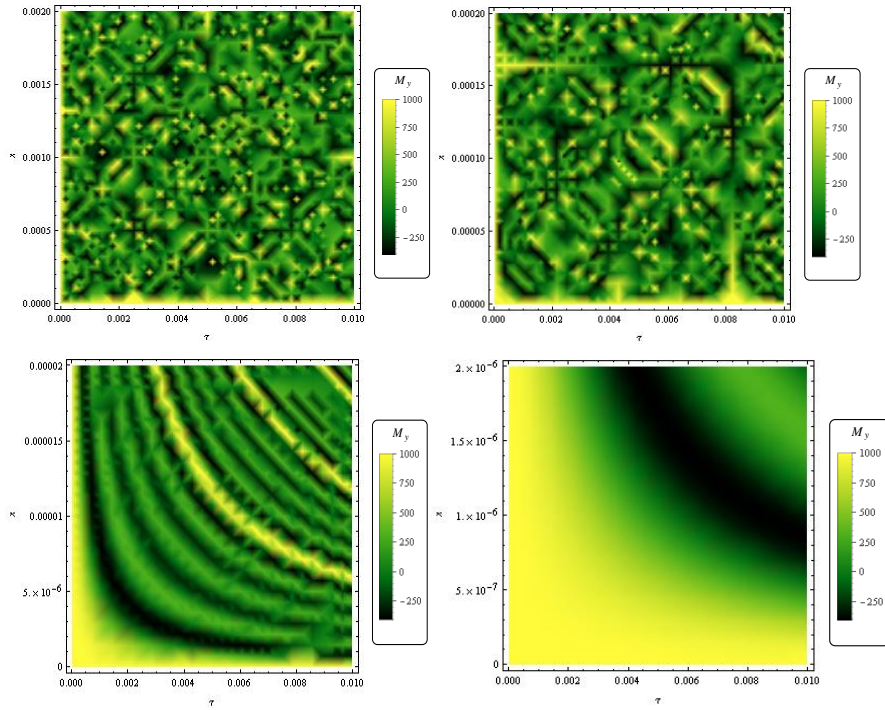
Fig. 4. Plots of M_y against x (for different geometrical ranges) for human liver [10] at 1.5T: C_1 = 1000, G = 0.2Tm^{-1}, τ = 2ms.
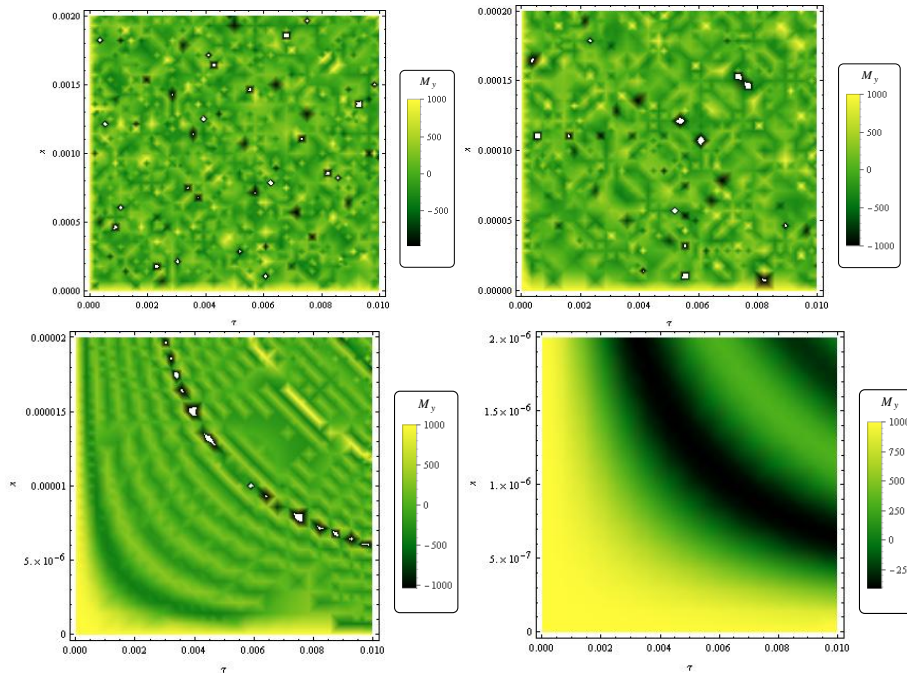
Fig. 5. Density plots of M_y against the gradient pulse duration and x (for different geometrical ranges) for normal breast fat [11] at 1.5T: $C_1 = 1000$, $G = 0.2Tm^{-1}$.

Fig. 6. Density plots of M_y against the gradient pulse duration τ and x (for different geometrical ranges) for fibroglandular tissues [11] at 1.5T: $C_1 = 1000$, $G = 0.2\text{Tm}^{-1}$.

Fig. 7. Density plots of M_y against the gradient pulse duration τ and x (for different geometrical ranges) for cancerous lesions [11] at 1.5T: $C_1 = 1000$, $G = 0.2\text{Tm}^{-1}$.

Fig. 8. Density plots of M_y against the gradient pulse duration τ and x (for different geometrical ranges) for human liver [11] at 1.5T: $C_1 = 1000$, $G = 0.2Tm^{-1}$[13].

x(m)	$\varepsilon = Cos(\gamma G\tau x)$	$P_0(\varepsilon) =$	$P_1(\varepsilon) = \varepsilon$	$P_2(\varepsilon) = \frac{1}{2}(3\varepsilon^2 -$	$P_3(\varepsilon) = \frac{1}{2}(5\varepsilon^3 - 3\varepsilon)$	$P_4(\varepsilon) = \frac{1}{8}(35\varepsilon^4 - 30\varepsilon^2 + 3)$
1.0	0.711661141	1	0.711661141	0.259692370	0.545241994	-0.402028850
1.0 x10^{-3}	0.862731119	1	0.862731119	0.616457474	1.173972117	0.007562160
1.0 x10^{-6}	0.994357171	1	0.994357171	0.983119274	1.960738556	0.944285000
1.0 x10^{-9}	0.999999994	1	0.999999994	0.999999983	1.999999960	0.999999944
1.0 x10^{-12}	1.000000000	1	1.000000000	1.000000000	2.000000000	1.000000000
1.0 x10^{-15}	1.000000000	1	1.000000000	1.000000000	2.000000000	1.000000000

Table 2. Geometrical behaviour of Legendre polynomials for arbitrary n. $\gamma = 2.6571 \times 108$ rad $T^{-1}s^{-1}$, $G = 0.2Tm^{-1}$, $\tau = 2ms$.

3   Fluid Velocity Computation

From equation (7), we write: $\dfrac{1}{v(x)}\left(T_0 + \dfrac{dv}{dx}\right) = \dfrac{1}{l\tan\dfrac{x}{l}}$ (20)

A solution to equation (20) is given as follows:

$$v(x) = |C_0|\sin\frac{x}{l} - T_0\left[l\ln\left(\sin\frac{x}{2l}\right) - l\ln\left(\cos\frac{x}{2l}\right)\right]\sin\frac{x}{l}$$ (21)

where $|C_0|$ is a constant. For $l = 9.41 \times 10^{-6}$m, we have the following expressions:

$v(x) = 0.84996126\,73843732\,|C_0| - T_0(0.0000046844\,30550178815\,3)$ (for x

= 20μm) (22)

$v(x) = 0.210971\,|C_0| + T_0(0.0000044421)$ (for x = 2μm) (23)

Tissue	$n = \dfrac{T_1}{T_2}$	n(n+1)	v (ms^{-1})	$|C_0|$	$\dfrac{|C_0|}{T_0}$	$\dfrac{|C_0|}{\sqrt{T_g}}$	M_{yn}
CSF	10.00000	110.0000	1.13474E-06	2.56E-05	5.81E-06	2.02267E-05	-240.356
White Matter	8.709677	84.56816	2.7958E-06	5.28E-05	5.88E-06	1.93364E-05	284.540
Grey Matter	8.070175	73.19791	3.39576E-06	5.83E-05	5.92E-06	1.88906E-05	47.6983
Kidney	10.12195	112.5758	3.39910E-06	7.79E-05	5.81E-06	2.0310E-05	-260.547
Liver	10.70175	125.2293	4.50896E-06	0.000111	5.79E-06	2.07035E-05	-130.436
Normal breast fat	4.166667	21.52778	1.65572E-05	0.000133	6.45E-06	1.63358E-05	-384.197
Fibroglandular tissue	8.75.000	85.31250	4.30459E-06	8.18E-05	5.87E-06	1.93644E-05	284.091
Cancerous lesions	8.000000	72.00000	3.92031E-06	6.66E-05	5.92E-06	1.88416E-05	3.89746
Cyst	2.626937	9.527738	4.62174E-06	2.41E-05	7.11E-06	1.59194E-05	447.473
Abscesses	5.709278	38.30514	2.99492E-06	3.4E-05	6.15E-06	1.7264E-05	343.137

Table 3. Values of the relaxation and fluid dynamic parameters for different tissues at 1.5T; γ = 2.6571 × 108 rad T^{-1}s^{-1}, G = 0.2Tm^{-1}, τ = 2ms, x = 20μm.

Tissue	$n = \dfrac{T_1}{T_2}$	n(n+1)	v (ms^{-1})	$|C_0|$	$\dfrac{|C_0|}{T_0}$	$\dfrac{|C_0|}{\sqrt{T_g}}$	M_{yn}
CSF	10.00000	110.0000	1.13474E-06	-8.72656E-05	-1.98331E-05	-6.89895E-05	92.5488
White Matter	8.709677	84.56816	2.79580E-06	-0.000176046	-1.95815E-05	-6.44243E-05	248.727
Grey Matter	8.070175	73.19791	3.39576E-06	-0.000191488	-1.94229E-05	-6.20137E-05	327.970
Kidney	10.12195	112.5758	3.39910E-06	-0.000266031	-1.98531E-05	-6.94029E-05	78.2675
Liver	10.70175	125.2293	4.50896E-06	-0.000382540	-1.99414E-05	-7.13311E-05	11.9889
Normal breast fat	4.166667	21.52778	1.65572E-05	-0.000356666	-1.72580E-05	-4.36825E-05	770.784
Fibroglandular tissue	8.750000	85.31250	4.30459E-06	-0.000272869	-1.95906E-05	-6.45727E-05	243.749
Cancerous lesions	8.000000	72.00000	3.92031E-06	-0.000218292	-1.94037E-05	-6.17423E-05	336.676
Cyst	2.626937	9.527738	4.62174E-06	-4.95343E-05	-1.45990E-05	-3.26691E-05	895.037
Abscesses	5.709278	38.30514	2.99492E-06	-0.000102279	-1.84893E-05	-5.19164E-05	611.207

Table 4. Values of the relaxation and fluid dynamic parameters for different tissues at 1.5T; γ = 2.6571 × 108 rad T^{-1}s^{-1}, G = 0.2Tm^{-1}, τ = 2ms, x = 2μm.

In tables (3-4), the values of the tissue velocities have been calculated from equation (10). The data is used to determine the values of the constant C_0. It is observed that equation (7) fits perfectly into the system as shown in equations (21) to (23). Using CSF as an example, a correlated expression to determine the constant is given as:

$$|C_0| = -1.98331 \times 10^{-5} T_0 = -6.89895 \times 10^{-5} \sqrt{T_g} \qquad (24)$$

This expression shows that the hemodynamic response of different tissues can be analyzed as a function of relaxation rates. Furthermore, velocity mapping can be done easily with these results and easily evaluated for different size of B$_0$ fields.

It is noteworthy from figures (5-8) that the best contrasts are obtained at 20μm; this is also confirmed in Tables (3-4). The results obtained in this study revealed that imaging at 20μm can be a very useful NMR signal delineation of cancerous lesions.

4   Conclusion

We have transformed the Bloch NMR flow equation to Legendre equation and obtained the NMR transverse magnetization in terms of the Legendre polynomials. Equation (15) does not change its form when -ε is substituted for ε. Hence, we are only interested in solutions of equation (15) which are even or odd functions of ε. Since ε → -ε implies that if we define $\theta = \frac{x}{l} \to \pi - \theta$ and z → - z the NMR transverse magnetization functions are symmetric or antisymmetric with respect to the *xy* plane. The parameter n, is the orbital angular momentum quantum number with integer values 0, 1, 2, 3, . . . , and the measured values of orbital angular momentum can only be 0, $2\hbar^2$, $6\hbar^2$, $12\hbar^2$,……… It is customary to designate the corresponding angular momentum states by the symbols S, P, D, *F*, . . . , which are familiar in atomic spectroscopy. If there are several particles in the NMR system, lower case letters *s, p, d,* . . . may be used to identify the angular momentum state of each particle, and capital letters S, P, D, will be reserved for the total orbital angular momentum. From tables (1-4), different tissue areas with different hemodynamic responses can be accurately reflected by the NMR transverse magnetization as represented by the Legendre polynomials. The spectroscopic display of transverse magnetization M_y, for different tissues are shown in figures (1-4) while figures (5-8) represent the density maps of transverse magnetization M_y, against the gradient pulse duration τ and x for different geometrical ranges for different tissues. These computational analyses can be very invaluable in functional Magnetic Resonance Imaging (fMRI), Magnetic Resonance Angiography (especially for imaging pulsating and non-uniform flow in blood vessels) and Magnetic Resonance Spectroscopy (MRS) to improve health care. It is observed in table (3) – (4) that some values of $\frac{|C_0|}{\sqrt{T_g}}$ for fibroglandular tissue and cyst appear (in bold) are suspected to carry specific information. These values will be investigated further for different brain tissues in our next studies.

References

1. Bammer R, Skare S, Newbould R, Liu C, Thijs V, Ropele S, Clayton DB, Krueger G, Moseley ME, Glover GH. Foundations of Advanced Magnetic Resonance Imaging. NeuroRx. 2005; 2(2): 167–196.
2. Awojoyogbe OB. Studies on the Application of Nuclear Magnetic Resonance (NMR, MRI) in the Estimation of Human Blood Flow Rates. Ph.D Thesis: Federal University of Technology, Minna, Nigeria (Unpublished) 1997.
3. Botnar R, Scheidegger MB, Boesiger P. Quantification of blood flow patterns in human vessels by magnetic resonance imaging. Tech. and Health Care 1996; 4: 97-112.
4. Abragam A. Principles of Nuclear Magnetism. Oxford University Press: London 1961.
5. Chaouachi A, Boubaker K, Amlouk M, Bouzouita H. Enhancement of pyrolysis spray disposal performance using thermal time-response to precursor uniform deposition. Eur. Phys. J. Appl. Phys. 2007; 37: 105-109.
6. Dada O.M., Awojoyogbe O.B., Adesola O.A. and Boubaker K. Magnetic Resonance Imaging-derived Flow Parameters for the Analysis of Cardiovascular Diseases and Drug Development. *Magnetic Resonance Insights* 2013; 6: 83–93.
7. O.B. Awojoyogbe O.M. Dada, K. Boubaker and O.A. Adesola. Flow Dynamics in Restricted Geometries: A Mathematical Concept Based on Bloch NMR Flow Equation and Boubaker Polynomial Expansion Scheme. *Journal of Applied Mathematics and Physics* 2013; 1: 71-78.
8. O.B. Awojoyogbe, M. Dada. Mathematical Design of a Magnetic Resonance Imaging Sequence Based on Bloch NMR Flow Equations and Bessel Functions. Chin J Magn Reson Imaging 2013; 4(5): 379-386.
9. Buxton RB. Introduction to Functional Magnetic Resonance Imaging: Principles and Techniques (2nd Edition). Cambridge University Press, Cambridge, United Kingdom. pp 155.
10. Brix G, Kolem H, Nitz WR, Bock M, Huppertz A, Zech CJ, and Dietrich O. Basics of MRI and Magnetic Resonance Spectroscopy. Springer Berlin Heidelberg, 2008, pp 17.
11. Hendrick, RE. Breast MRI: Fundamentals and Technical Aspects. Springer; New York, USA. 2008.
12. Yilmaz UN, Yaman F and Atilgan SS. MR T1 and T2 relaxations in cysts and abscesses measured by 1.5 T MRI. Dentomaxillofacial Radiology 2012; 41: 385–391.
13. Price WS. Pulsed Field Gradient Nuclear Magnetic Resonance as a Tool for Studying Translational Diffusion: Part I. Basic Theory. Concepts Magn. Reson. 1997; 9: 299-336.